A Systematic Theoretical Study on Electronic Interaction in Cu-based Single-Atom Alloys

Guo-Chen Zhao, Yongqing Qiu, and Chun-Guang Liu*

Read Online

ACCESS | Metrics & More | Article Recommendations | SI Supporting Information

ABSTRACT: A meticulous understanding of the electronic structure of catalysts may provide new insight into catalytic performances. Here, we present a $d-d$ interaction model to systematically study the electronic interaction in Cu-based single-atom alloys. We refine three types of electronic interactions according to the position of the antibonding state relative to the Fermi level. Moreover, we also find a special phenomenon in Mn-doped single-atom alloys in which no obvious electronic interaction is found, and the doped Mn metal seems to be a free atom. Then, taking Hf/ Mn-doped single-atom alloys as an example, we discuss the electronic structure based on the density of states, charge transfer, crystal orbital Hamilton population, and wavefunctions. To support the proposed model and help analyze the data, we perform an energetic analysis of water dissociation in the water-gas shift reaction. The calculation results well confirm the $d-d$ interaction model, where alloys with the position of the antibonding state close to the Fermi level exhibit excellent water dissociation ability in the water-gas shift reaction. However, the catalytic performance of the Mn-doped alloy is unsatisfactory, which is caused by its own special phenomenon.
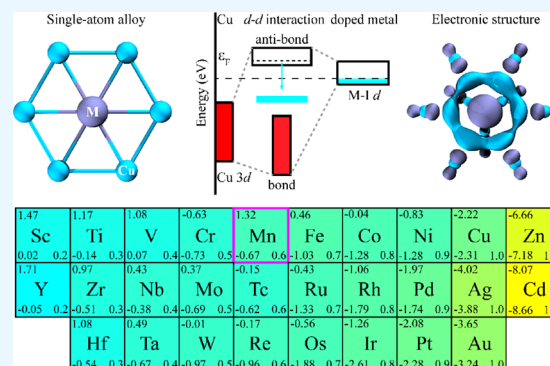
INTRODUCTION

The d-band model, which was proposed in 1995, has been well demonstrated to develop a quantitative understanding of trends in transition-metal catalysis[1−3] and has been employed as a descriptor of the design scale relationship in many catalytic reactions.[4−6] In this model, its essence is an adsorbate bonding model evolved from the Newns−Anderson−Grimley model to describe the hybridization between adsorbate molecules and electronic band structures of metal surfaces.[7−10] It is well known that adsorbate molecules over the metal surface would lead to an orbital interaction between the s/p orbitals of adsorbate molecules and the d orbital of metal surface, thus causing energy level splitting. The position of the antibonding state relative to the Fermi level plays a crucial role in chemisorption and catalytic property. The d-band center of the antibonding state can be viewed as a key parameter to predict the position of the antibonding state. Therefore, tuning the d-band center may be an effective strategy to design new catalysts. Until now, for specific metals, there have been usually two methods to regulate the d-band center of the material itself, one is to control the coordination number, and the other is to adjust the lattice strain. For example, Tian et al. illustrated the synergistic effects derived from both the lattice strain and ligand effects in the catalysts and revealed the existence of fewer strongly bonded platinum-oxygen sites.[11] Wang et al. reported on a strategy to resolve the problems of the interfacial reconstructions and nanocatalyst geometries by exploiting intrinsic surface stresses in two-dimensional transition-metal nanosheets.[12]

Nowadays, alloying is an emerging strategy to harmonize the electronic structure of metal catalysts. However, conventional alloy catalysts lack precise control over the catalysts with several types of active sites or local binding environments for different intermediates.[13,14] Meanwhile, mean-field behavior in metals often dominates the adsorption property of heterogeneous catalysts and restricts their achievable catalytic properties.[15] Single-atom alloys (SAAs) can bridge homogeneous and heterogeneous catalysis, thus effectively tailoring the optimal active site of catalysts.[16−18] The varieties of electronic structures typically observed on alloying involve a shift of the d-band position relative to the Fermi level. Greeley et al. designed the alloy catalysts from first-principles calculations, highlighting the function of the d-band center and the differing coupling matrix elements of the hosts.[19,20] Currently, Cu-based catalysts appeared in many industrial processes with fascinating catalytic properties, such as the water-gas shift reaction (WGSR),[21,22] CO_2 reduction reaction,[23−25] and so on.

Figure 1. Schematic illustrations of $d-d$ interaction between the doped metal and host metal correspond to M-I (a), M-II (b), and M-III (c) alloys, respectively. The rectangular frame represents the d orbital of the metal. The color fill in the rectangular frame represents the electron filling in the d orbital, where red fill represents the host metal and cyan the doped metal. (d) Part of periodic table shows the d-band center varieties of CuM on alloying.

Furthermore, a series of studies have also shown that Cu-based SAAs exhibit excellent catalytic abilities[26−28] in many reactions, nevertheless, this does not mean a thorough understanding of the origin on catalytic performances. Previous research studies were focused on experimental science and macroscopic theoretical research studies, whereas the detailed electronic structure on the surface of Cu-based SAAs is still lacking. To date, the role of electronic interaction between the doped metal and host metal in surface chemisorption and catalysis has not been disclosed until now.

In this work, we studied 27 Cu-based SAAs and meticulously discussed the electronic interaction by first-principles calculations. According to the electronic interaction between the doped metal and host metal, Cu-based SAAs studied here were divided into three sets. Surprisingly, we found a unique phenomenon that there is almost no electronic interaction in Mn-doped SAAs. Then, we conducted detailed electronic structure analysis including density of states (DOS), charge transfer, crystal orbital Hamilton population, and wavefunctions. Moreover, we performed an energetic analysis on water dissociation in the WGSR for the differences caused by the modification of the electronic structure. The calculation results show an obvious scaling relationship from the qualitative analysis between the electronic structure and catalytic performance, which fits the $d-d$ interaction model.

METHODS

The Vienna ab initio simulation package[29,30] is used in all spin polarization calculations with the generalized gradient approximation (GGA). We took the Perdew−Burke−Ernzer-hof functional[31] and projector augmented wave method.[32,33] The electronic states were expended on a plane wave basis with a kinetic cut-off energy of 400 eV. The convergence criterion was set as 1.0×10^{-5} eV in energy, and the force convergence criterion was set as 0.02 eV/Å. The transition state geometry optimizations are allowed to relax until the force on each atom is less than 0.02 eV/Å by the climbing-image nudged elastic band method.[34,35] Electronic structure and electronic factor analysis were calculated by Bader charge analysis software,[36] crystal orbital Hamilton population (COHP) analysis with the LOBSTER code,[37] and wavefunction analysis with the VASPMO code.[38]

We selected the Cu(111) facet as the calculation model because of its typical benchmark for fundamental studies.[39−41] The slab is a 4×4 unit cell with four layers fixing the bottom two layers and separated by 15 Å of vacuum region. The structure relaxation sampling of the k-point Gamma scheme is $3 \times 3 \times 1$, and the DOS calculation is $7 \times 7 \times 1$. All the Gibbs free energy (ΔG) calculations were corrected at 523 K and 100 kPa (experimental conditions reported by Nakamura et al.)[42] by the VASPKIT program.[43]

RESULTS AND DISCUSSION

***d−d* Interaction Model.** For electron interaction between metals, it is generally attributed to the interaction between metal d orbitals. Then, the energy level after electron interaction will split into a bonding state and an antibonding state via interactions of metal d orbitals. The Fermi level plays a vital role to stabilize the system, where the position of the antibonding state relative to it directly regulates the electronic

Figure 2. Electronic structures of Cu and CuHf. The DOS diagrams correspond to Cu and CuHf (a), Cu and Hf metals in CuHf (b), Cu metal in CuHf (c), and Hf metal in CuHf (d), respectively. The COHP analysis of Cu−Cu bond (e) and Cu−Hf bond (f) indicates the hybridization between the doped metal and host metal. (g) Charge density difference reveals the charge transfer in CuHf, in which the yellow and cyan isosurfaces (isosurface levels: 0.002) stand for the accumulation and depletion of electron density, respectively. (h) Wavefunctions of bonding and antibonding states for CuHf illustrate the real-space bonding formed.

interaction. The higher the position of the metal d state relative to the Fermi level, the higher the d-band center and the narrower the metal valence band; conversely, the lower the position of the metal d state relative to the Fermi level, the lower the d-band center, the wider the metal valence band. Here, we present a $d-d$ interaction model in an attempt to explore the electronic interaction in Cu-based SAAs (labeled CuM, where M represents doped metal). To understand surface science more intuitively, we mainly focus on surface-localized metal in our ensuing studies. The $d-d$ interaction model, as in Figure 1, reveals a striking feature of the electronic interaction between the doped metal and host metal (Cu) in CuM. We select the most close-packed surface of the doped metal (state before interaction) and doped metal of CuM (state after interaction) to simulate the varieties on alloying. The model exhibits three electronic interactions, corresponding to three alloy sets according to the varieties of d state in doped metal on alloying: (I) M = Hf, Ta, Zr, Ti, Y, Nb, W, Sc, Mo, Re, V; (II) M = Tc, Os, Ru, Cr, Co, Fe, Rh, Ni, Ir; and (III) M = Cd, Zn, Au, Pt, Ag, Pd. The positions of the d states of M-I, M-II, and M-III alloys after electron interaction relative to the Fermi level are divided into three types: (I) The doped

metal d state is completely above the Fermi level; (II) the doped metal d state is partially above the Fermi level; and (III) the doped metal d state is completely below the Fermi level, respectively. We rely on the d-band center to qualitatively and intuitively describe the varieties of the d state in CuM, which are summarized in Figure 1d (see Table S1 for details in the Supporting Information).

Clarifying the main contribution of bonding and antibonding states split by electronic interaction between the doped metal and host metal will play a guiding role for us to better explain the $d-d$ interaction model. It can be seen intuitively from the DOS analysis, the main contribution of the bonding state comes from the host metal, whereas the doped metal controls the antibonding state. More detailed DOS analysis will be shown in the Electronic Structure section later. On the basis of understanding the main contribution of bonding and antibonding states (see the subsequent Electronic Structure section), we continue to explain the $d-d$ interaction model.

Electronic Interaction of the M-I Alloy. As shown in the schematic diagram in Figure 1a, the electronic interaction results in the formation of a bond (host metal d state) and an antibond (doped metal d state) on alloying. As mentioned

above, the position of the antibonding state relative to the Fermi level plays a crucial role in chemisorption and catalytic property. It can be seen that the antibonding state for the M-I alloy is the highest relative to the Fermi level in three electronic interactions, and the doped metal d state is completely above the Fermi level after the electron interaction. Before the electron interaction, the doped metal d state of the M-I alloy is partially above the Fermi level, where the d orbital partially occupies electrons. The position of the doped metal d state for M-I alloying relative to the Fermi level is higher than that before the electronic interaction, the higher the d-band center and the narrower the metal valence band. However, the orbital volume of the metal itself cannot be changed, in order to make the unoccupied orbitals of the metal free of filling electrons, electrons above the Fermi level (d state of the antibonding state) will be completely transferred to below the Fermi level after the electron interaction. At this time, the antibonding orbital approximates an empty d orbital, and the bonding orbital completely occupies electrons. It is an ideal electronic structure for catalysts. It means that the electronic interaction of the M-I alloy may make catalytic activity enhanced compared to that of M-II and M-III alloys.

Electronic Interaction of the M-II Alloy. The electronic interactions of the M-II alloy and M-I alloy are similar to some extent, the difference is that the doped metal d orbital of the M-II alloy occupies more electrons than the M-I alloy before the electronic interaction. This difference leads to the fact that the doped metal d state of the M-II alloy cannot be completely above the Fermi level after the electron interaction. Therefore, the doped metal d state of M-II alloy can only be partially above the Fermi level, causing electrons above the Fermi level to be fully transferred to below the Fermi level after the electron interaction. At this time, the antibonding orbital partially occupies electrons, and the bonding orbital still completely occupies electrons. It is noted that according to our calculation results, the bonding orbital of the M-II alloy (host metal Cu) does not downshift after the electron interaction, but upshift slightly compared to the M-I alloy. Although the bonding orbital upshifts, it does not exceed the Fermi level, and the bonding orbital always remains fully filled with electrons. This phenomenon cannot greatly affect the activity of metal catalysts, because the activity of metal catalysts mainly depends on the contribution of the antibonding state. Thereby, the catalytic activity of the M-II alloy may still be improved, but the effect may not be as good as that of the M-I alloy.

Electronic Interaction of the M-III Alloy. The M-III alloy exhibits a completely different electron interaction than M-I and M-II alloys. It can be seen that the antibonding state for the M-III alloy is the lowest relative to the Fermi level in three electronic interactions, and the doped metal d state is completely below the Fermi level after the electron interaction. Although the antibonding state of the M-III alloy upshifts like M-I and M-II alloys, the doped metal d state does not exceed the Fermi level. In the process of electron interaction, including bonding state and antibonding state, the phenomenon of electrons crossing the Fermi level does not occur in the whole alloy. The bonding and antibonding orbitals of the M-III alloy always occupy all electrons during the electron interaction. Therefore, solely relying on the contribution of the antibonding state does not seem to improve the activity of the catalyst. At this time, the downshift of the bonding state will promote the activity of the metal catalyst. Because the contribution of the bonding state has little effect on the

metal catalyst, it is possible that the catalytic activity of the M-III alloy is only slightly improved compared to that of M-II and M-III alloys.

In short, we summarize three electron interactions in the d–d interaction model. Surprisingly, we discover a special alloy in which CuMn alloy cannot be explained by this model. The doping of Mn atom in the host metal Cu does not seem to show significant electronic interactions, where the doped Mn metal is more like a free atom. The specific reason will be explained in detail in the Electronic Structure section.

Electronic Structure. To reveal the essence of electronic interaction, we conducted a rigorous study on the electronic structure. Taking Cu and CuHf as examples, we show the DOS analysis in Figure 2. According to previous description, we first consider the main contribution of bonding and antibonding states. We can clearly see the sharp contrast between the bonding state and antibonding state, where the former belongs to host metal (Cu) and the latter is classified by doped metal (Hf) from Figure 2a–d. As shown by the electronic interaction in Figure 2c,d, the DOS of host metal Cu deviates from the Fermi level, while that of doped metal Hf splits into two parts, a downshifted and an upshifted part. It is observed that the contribution of the bonding state can be divided into two components, a lush peak of Cu metal and a dwarf peak of Hf metal below the Fermi level. Because of the energetic and spatial overlap between both, the bonding state forms, but the contribution of which mainly depends on Cu metal, owing to its absolute component. Relatively, the peak above the Fermi level of Hf metal corresponds to the contribution from an antibonding state. At this point, we have a deep understanding on the contribution of bonding and antibonding states.

To further explore the origin of electronic interaction, we investigated the d state of CuHf in the framework of crystal field theory. The d states of Cu and Hf metals are both split by strong interaction with their coordination environment, in which d_{xz} and d_{yz} orbitals are a set of degenerate orbitals as are d_{xy} and $d_{x^2-y^2}$ orbitals. Corresponding to the d–d interaction model, the maximum decrease of energy level represents d_{xz} and d_{yz} orbitals of Cu metal, while the maximum increase denotes d_{xz} and d_{yz} orbitals of Hf metal (Table S2). In terms of electronic factor, primitive electrons filled in d_{xz} and d_{yz} orbitals of Hf metal transfer to below the Fermi level, which are stored in d_{xy} and $d_{x^2-y^2}$ orbitals. Therefore, the fundamental of energetic and spatial overlap between Cu and Hf metals appeared, which is the hybridization of d_{xy} and $d_{x^2-y^2}$ orbitals between both. However, because of the mismatching orbital symmetry between Cu and Hf metals, the d_{z2} orbital shows a weak hybridization with little contribution. From the charge density difference analysis in Figure 2g and Bader charge analysis in Figure S1, we can clearly see the electrons transfer around Hf metal, which is consistent with the analysis in the framework of crystal field theory.

We further investigated some important factors responsible for the modification of d-band properties in CuHf, which examines the strain and ligand effects. The synergy between strain and ligand effects leads to the evolution of the electronic structure, in which the ligand effect dominates. On the strain aspect (lattice parameter), the shortening of the distance between host metals and doped metal means that the compression strain will increase the d orbital overlap between host metals and doped metal, resulting in a downshift of the d-band center for host metals and doped metal. As a complement of strain effect, we built a Cu model with the same strain of
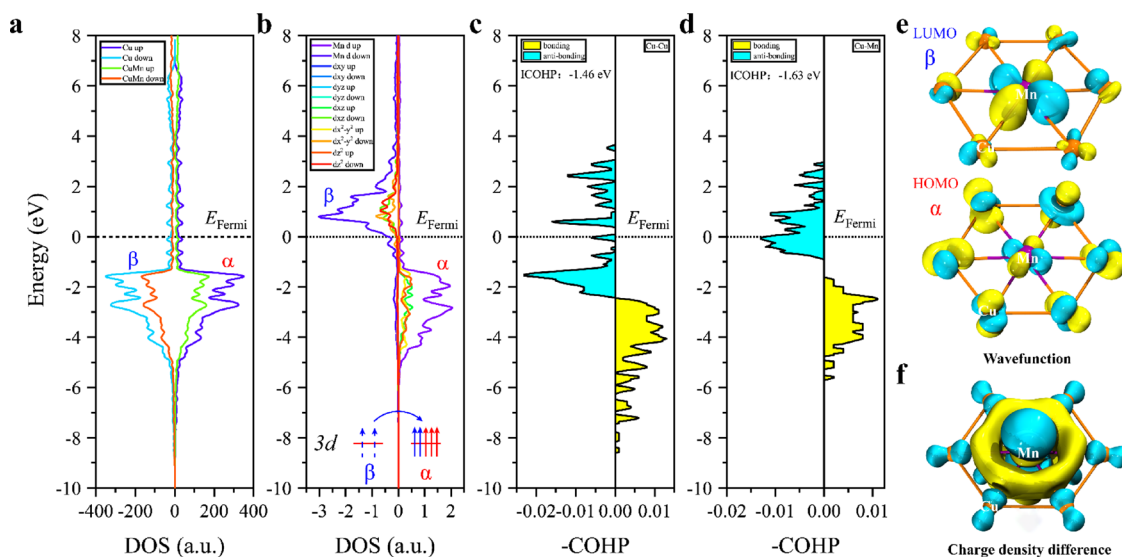
Figure 3. Electronic structures of Cu and CuMn. The DOS diagrams correspond to Cu and CuMn (a) and Mn metal in CuMn (b), respectively. The COHP analysis of Cu−Cu bond (c) and Cu−Mn bond (d) indicates the similarity between Cu and CuMn. (e) Wavefunctions of the α-spin and β-spin d state in CuMn illustrate the real-space bonding formed. (f) Charge density difference reveals the charge transfer in CuMn, in which the yellow and cyan isosurfaces (isosurface levels: 0.002) stand for the accumulation and depletion of electron density, respectively.

CuHf by fixing the bond length of the Cu surface (denoted Cu with strain). The results show that strain effect weakens the d orbital overlap of the central Cu atom and surrounding six surface Cu atoms, upshifting both of the d-band center (Table S3). On the ligand aspect (coordination environment), strong hybridization with electronic interaction makes a downshift and an upshift of the d-band center for Cu and Hf metals, respectively. To gain deep insights into the strong orbital hybridization quantitatively, we performed the COHP analysis for the Cu−Hf bond and Cu−Cu bond (Figure 2e,f). Note that a more negative value of integrated-crystal orbital Hamilton population (ICOHP) implies a stronger orbital hybridization (−4.35 vs −1.46 eV). Also, the d state nature of bonding and antibonding states becomes even clearer when one looks at the spatial distribution of wavefunctions in CuHf, which are more deeply rooted in terms of both shape and spatial extent (Figure 2h). The observed bonding nature results from two main contributions: ionic and covalent bonding. The increased negative charge density on the impurity ion (Hf) influences the ionic contribution, whereas the pi bond influences the covalent contribution and no effective sigma bond contribution is observed.

Next, we focus on CuMn. As shown in Figure 3a, except for the weaker d state peak of CuMn, there is almost no difference in the DOS shape of CuMn and Cu as shown in Figure 3a. The highly similar electronic structure means that CuMn may have unfriendly catalytic activity similar to that of pure Cu catalysts. Meanwhile, doped metal Mn forms a strong spin polarization because of its magnetic property. It is surprisingly found that the d state of host metal has hardly changed and the d-band center is not even shifted (Table S1). Moreover, α-spin d states of Cu and Mn metals are well matched because of the strong spin polarization of Mn metal with the downshift of the α-spin d state and upshift of the β-spin d state (Figure 3b, Table S4). However, the d-band property indicates that there are no prominent efficacious electron density mixing between the Mn metal α-spin d state and Cu metal α-spin d state. This may be expected from the d-band center position but cannot be completely relied upon. To further confirm this phenomenon,

we performed the COHP analysis in Figure 3c,d. The Cu−Mn bond is almost the same as the Cu−Cu bond, and the ICOHP differs only 0.17 eV. Coupled with a nearly uniform coordination field (five degenerate α-spin d orbitals of Cu and Mn metals in energy), special electronic structure features reveal the fundamental cause of Mn metal d state, which is similar to be free atom (Table S5). From the wavefunctions of α-spin and β-spin d orbitals in CuMn, we can intuitively see a special phenomenon mentioned above and almost no electron density mixing in Figure 3e.

A series of calculations reveals that this phenomenon occurs when the solute exhibits weak interactions with the electronic state of the matrix element at dilute concentrations (that is, in the absence of solute−solute bonding). This effect arises due to the minimal energy and spatial overlap between the solute and matrix atoms. Although the electronic structure is similar to be free atom in terms of its energy distribution, the equilibration of electron chemical potentials with the surrounding matrix gives the doped metal Mn a cationic character, as apparent from our calculations in Figures 3f and S1. The d orbital electron configuration of the Mn element is d^5, and its d orbital occupies five electrons as a whole, which means that α-spin and β-spin in the d orbital of the Mn element jointly occupy these five electrons. It is found that the d orbital of Mn metal in the CuMn alloy is also filled with five electrons, which can be obtained from our calculation results by magnetic moment (mag) analysis (approximately 4.6 μB on Mn metal). Although the number of d orbital electron fillings of Mn atoms before and after alloying remains the same, the electron filling ways of the two are quite different. From the DOS analysis, we can see the upshift of the β-spin d state and the downshift of the α-spin d state for the doped metal Mn in the CuMn alloy. The β-spin d state of the doped Mn is completely above the Fermi level, and the α-spin d state of the doped Mn is completely below the Fermi level. Because the unoccupied orbital does not allow electrons to be filled, the original electrons in the β-spin d state of the doped Mn will be transferred to below the Fermi level and stored by the α-spin d state of the doped Mn. At this time, the α-spin d state of the
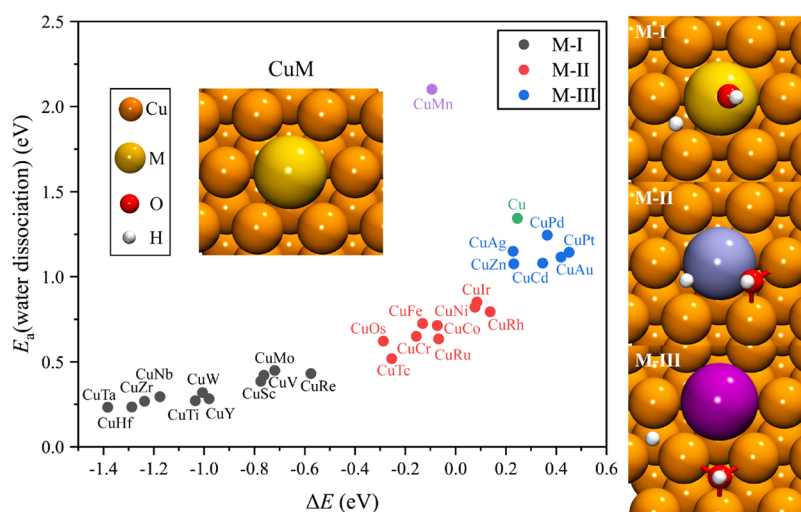
Figure 4. DFT-calculated activation energy (E_a) and reaction energy (ΔE) for Cu and CuM on water dissociation. The Cu, M (doped atom), O, and H are illustrated as orange, dark yellow, red, and white balls, respectively.

doped Mn is completely filled with electrons, while the β-spin d state of the doped Mn approximates an empty state. The α-spin and β-spin d states for the doped metal Mn in the CuMn alloy are similar to the antibonding state upshift and electron transfer phenomenon in the $d-d$ interaction model mentioned above. However, the d state of host metal Cu as a bonding contribution hardly changed its electronic structure before and after alloying, so the special phenomenon cannot be regarded as electronic interaction.

Furthermore, we found other strong spin-polarized systems like CuCr, CuCo, and CuFe; however, they do not have the same trend as CuMn. The varieties of d states in the doped metal on alloying for CuCr, CuCo, and CuFe prefer the M-II alloys in the $d-d$ interaction model.

Role of the d State in Catalysis. To explore the role of the d state in catalysis, we employed the WGSR (CO + H$_2$O → CO$_2$ + H$_2$) as an example to support the proposed model and help analyze the data. In catalytic reactions, the stability of catalysts is crucial. Before exploring their catalytic activity, it is essential to analyze the stability of these catalysts. We examined the difference in stability of the alloyed CuM relative to the pristine pure Cu catalyst, indicating that almost all doped M atoms assumed to be an adsorbate are thermodynamically stable when surrounded by host metal Cu, except CuZn, CuAg, and CuCd SAAs (Figure S2). Then, we compared the catalytic property of CuM with Cu by water dissociation, which is the rate-determining step.[21,22] Our calculated activation barrier on Cu (1.34 eV) is consistent with the experimental results of 1.23 eV[41] and the density functional theory (DFT)-GGA calculation results of 1.36 eV by Gokhale et al.[39] on the Cu(111) surface. Moreover, our results show that all activation barriers of water dissociation on M-I, M-II, and M-III alloys are less than that on Cu (except for the special CuMn), showing that alloying greatly enhances the water dissociation activity of Cu catalysts. We must point out that the catalytic behavior of the rate-determining step alone is not enough to quantitatively judge the catalytic property of the whole WGSR. Nonetheless, one can still rely on some special behavior to explain the catalytic activity like the relationship between the electronic structure and catalytic performance, including the electronic interaction between the doped atom and host atom on the catalyst surface, the strain and ligand

effects, and so on. As expected, from the qualitative analysis between the electronic structure and catalytic performance, the calculated results show a clear scaling relationship, which fits the $d-d$ interaction model. Based on electronic interaction, M-I alloys exhibit extraordinary catalytic performance with a slight activation energy and reaction energy, followed by M-II and M-III alloys (Figure 4). Furthermore, we can see that the special phenomenon in CuMn alloy leads to catalytic behavior as inactive as pure Cu or even worse than pure Cu in water dissociation. It is clear that the catalytic behavior of CuMn alloy is quite different from that of M-I, M-II, and M-III alloys, completely deviating from the above scaling relationship. It is consistent with our analysis results that the $d-d$ interaction model is not suitable for explaining CuMn alloys. The reason for this special phenomenon is due to the d state transition from fully filled state of pure Cu metal to half-filled state of the CuMn alloy. Therefore, it is inappropriate to correlate the catalytic behavior of the CuMn alloy with the efficiency for the WGSR in terms of water dissociation.

To evaluate the strain and ligand effects, we calculated the water dissociation process of Cu (1.34 eV), Cu with strain (1.11 eV), and CuHf (0.23 eV) in Table S6. Cu with strain simulates the strain effect, and CuHf simulates the synergistic effect of strain and ligand effects, indicating that both strain and ligand effects are aggressive and ligand effect is the domination, which is consistent with electronic structure analysis. Besides that, we also studied the geometric structure of key intermediates in water dissociation. In many cases, the decrease of the activation barrier is not enough as it might also result in increased adsorbate-catalyst interaction, leading to catalyst poisoning, which can be observed in the results for OH* adsorption energy in Table S7. Generally, the electronic structure is closely associated with the geometric structures. Then, we examined a series of geometric structures for water dissociation and found that the H$_2$O molecule prefers to adsorb on top site of doped metal, except for Au and Pt metals on the Cu metal top site (Figure S3). The transition state structure (Figure S4) is not much different from the H$_2$O* structure; however, the most interesting aspect is the difference in the active sites of water dissociation (H* + OH* in Figure S5). It is not difficult to note that M-I, M-II, and M-III alloys possess well-defined dissociative active sites, where OH*

prefers to dissociate on doped metal, between doped metal and host metal, and around host metal, respectively. It can be summarized as that the dissociative active site ranges from doped metal sole adsorption, to doped metal and host metal coadsorption, and finally to host metal co-adsorption for OH*, respectively. Also, OH* absorbs between Mn and Cu metals similar to host metal coadsorption because of the special d state of Mn metal like a free atom.

CONCLUSIONS

The $d−d$ interaction model plays a guiding role in the meticulous understanding of electronic interaction. Relying on the varieties of d-band centers for doped metal, three types of Cu-based SAAs are proposed. Furthermore, it was found that the rare Mn atom seems to be a free atom without almost electronic interaction on alloying. Detailed electronic structure analysis clarifies the fundamental of the electronic interaction between the doped metal and host metal in Cu-based SAAs. In the WGSR, alloys with an antibonding state above the Fermi level generally display an outstanding water dissociation activity. The special phenomenon that no obvious electronic interaction is observed in CuMn alloy restricts the catalytic activity of the water dissociation, and even the activation energy is higher than that of pure Cu catalysts. Furthermore, we investigated the geometric structure of key intermediates, and the results show that the adsorption site of OH* obeys the electronic interaction model.

ASSOCIATED CONTENT

Ⓢ Supporting Information

The Supporting Information is available free of charge at https://pubs.acs.org/doi/10.1021/acsomega.2c05536.

> The varieties of d-band centers, the energy levels of d orbitals, optimized structures, and DFT-calculated energies for CuM (PDF)

AUTHOR INFORMATION

Corresponding Author

Chun-Guang Liu − *Department of Chemistry, Faculty of Science, Beihua University, Jilin City 132013, P. R. China;* orcid.org/0000-0002-1220-5236; Email: liucg407@163.com

Authors

Guo-Chen Zhao − *Datang Northeast Electric Power Test & Research Institute, China Datang Corporation Science and Technology Research Institute, Changchun 130102, P. R. China;* orcid.org/0000-0001-9117-2622

Yongqing Qiu − *Institute of Functional Material Chemistry, Faculty of Chemistry, Northeast Normal University, Changchun 130024, P. R. China;* orcid.org/0000-0003-1027-8869

Complete contact information is available at:
https://pubs.acs.org/10.1021/acsomega.2c05536

Author Contributions

G.-C.Z. contributed to theoretical calculations, data processing, and manuscript writing.

Notes

The authors declare no competing financial interest.

REFERENCES

(1) Hammer, B.; Norskov, J. K. Why Gold is the Noblest of All the Metals. *Nature* **1995**, *376*, 238−240.
(2) Nørskov, J. K.; Abild-Pedersen, F.; Studt, F.; Bligaard, T. Density Functional Theory in Surface Chemistry and Catalysis. *Proc. Natl. Acad. Sci. U. S. A.* **2011**, *108*, 937−943.
(3) Nørskov, J. K.; Studt, F.; Abild-Pedersen, F.; Bligaard, T. *Fundamental Concepts in Heterogeneous Catalysis*. Wiley: Hoboken, New Jersey, 2014.
(4) Vojvodic, A.; Nørskov, J. K. New Design Paradigm for Heterogeneous Catalysts. *Natl. Sci. Rev.* **2015**, *2*, 140−143.
(5) Medford, A. J.; Vojvodic, A.; Hummelshøj, J. S.; Voss, J.; Abild-Pedersen, F.; Studt, F.; Bligaard, T.; Nilsson, A.; Nørskov, J. K. From the Sabatier Principle to a Predictive Theory of Transition-Metal Heterogeneous Catalysis. *J. Catal.* **2015**, *328*, 36−42.
(6) Feng, Y.; Shao, Q.; Ji, Y.; Cui, X.; Li, Y.; Zhu, X.; Huang, X. Surface-Modulated Palladium-Nickel Icosahedra as High-Performance Non-Platinum Oxygen Reduction Electrocatalysts. *Sci. Adv.* **2018**, *4*, No. eaap8817.
(7) Anderson, P. W. Localized Magnetic States in Metals. *Phys. Rev.* **1961**, *124*, 41−53.
(8) Newns, D. M. Self-Consistent Model of Hydrogen Chemisorption. *Phys. Rev.* **1969**, *178*, 1123−1135.
(9) Vojvodic, A.; Nørskov, J. K.; Abild-Pedersen, F. Electronic Structure Effects in Transition Metal Surface Chemistry. *Top. Catal.* **2014**, *57*, 25−32.
(10) Hammer, B. JK Nørskov in Advances in catalysis, 2000; Vol. *45*, pp 71−129.
(11) Tian, X.; Zhao, X.; Su, Y. Q.; Wang, L.; Wang, H.; Dang, D.; Chi, B.; Liu, H.; Hensen, E. J. M.; Lou, X. W.; Xia, B. Y. Engineering Bunched Pt-Ni Alloy Nanocages for Efficient Oxygen Reduction in Practical Fuel Cells. *Science* **2019**, *366*, 850−856.
(12) Wang, L.; Zeng, Z.; Gao, W.; Maxson, T.; Raciti, D.; Giroux, M.; Pan, X.; Wang, C.; Greeley, J. Tunable Intrinsic Strain in Two-Dimensional Transition Metal Electrocatalysts. *Science* **2019**, *363*, 870−874.
(13) Wang, Y.; Cao, L.; Libretto, N. J.; Li, X.; Li, C.; Wan, Y.; He, C.; Lee, J.; Gregg, J.; Zong, H.; Su, D.; Miller, J. T.; Mueller, T.; Wang, C. Ensemble Effect in Bimetallic Electrocatalysts for CO_2 Reduction. *J. Am. Chem. Soc.* **2019**, *141*, 16635−16642.
(14) Ai, X.; Zou, X.; Chen, H.; Su, Y.; Feng, X.; Li, Q.; Liu, Y.; Zhang, Y.; Zou, X. Transition Metal-Boron Intermetallics with Strong Interatomic d-sp Orbital Hybridization for High-Performing Electrocatalysis. *Angew. Chem., Int. Ed.* **2020**, *59*, 3961−3965.
(15) Greiner, M. T.; Jones, T. E.; Beeg, S.; Zwiener, L.; Scherzer, M.; Girgsdies, F.; Piccinin, S.; Armbrüster, M.; Knop-Gericke, A.; Schlögl, R. Free-Atom-Like d States in Single-Atom Alloy Catalysts. *Nat. Chem.* **2018**, *10*, 1008−1015.
(16) Kyriakou, G.; Boucher, M. B.; Jewell, A. D.; Lewis, E. A.; Lawton, T. J.; Baber, A. E.; Tierney, H. L.; Flytzani-Stephanopoulos, M.; Sykes, E. C. H. Isolated Metal Atom Geometries as a Strategy for Selective Heterogeneous Hydrogenations. *Science* **2012**, *335*, 1209−1212.
(17) Tierney, H. L.; Baber, A. E.; Kitchin, J. R.; Sykes, E. C. H. Hydrogen Dissociation and Spillover on Individual Isolated Palladium Atoms. *Phys. Rev. Lett.* **2009**, *103*, No. 246102.
(18) Gu, K.; Wei, F.; Cai, Y.; Guo, H. Dynamics of Initial Hydrogen Spillover from a Single Atom Platinum Active Site to the Cu(111) Host Surface: The Impact of Substrate Electron-Hole Pairs[J]. *J. Phys. Chem. Lett.* **2021**, *12*, 8423−8429.
(19) Greeley, J.; Mavrikakis, M. Alloy Catalysts Designed from First Principles. *Nat. Mater.* **2004**, *3*, 810−815.

(20) Greeley, J.; Nørskov, J. K.; Mavrikakis, M. Electronic Structure and Catalysis on Metal Surfaces. *Annu. Rev. Phys. Chem.* **2002**, *53*, 319−348.

(21) Wang, Y. X.; Wang, G. C. A Systematic Theoretical Study of Water Gas Shift Reaction on Cu(111) and Cu(110): Potassium Effect. *ACS Catal.* **2019**, *9*, 2261−2274.

(22) Rodriguez, J. A.; Remesal, E. R.; Ramírez, P. J.; Orozco, I.; Liu, Z.; Graciani, J.; Senanayake, S. D.; Sanz, J. F. Water-Gas Shift Reaction on K/Cu(111) and Cu/K/TiO$_2$(110) Surfaces: Alkali Promotion of Water Dissociation and Production of H$_2$. *ACS Catal.* **2019**, *9*, 10751−10760.

(23) Gao, D.; Arán-Ais, R. M.; Jeon, H. S.; Cuenya, B. R. Rational Catalyst and Electrolyte Design for CO$_2$ Electroreduction towards Multicarbon Products. *Nat. Catal.* **2019**, *2*, 198−210.

(24) Zhuang, T. T.; Liang, Z. Q.; Seifitokaldani, A.; Li, Y.; De Luna, P.; Burdyny, T.; Che, F.; Meng, F.; Min, Y.; Quintero-Bermudez, R.; Dinh, C. T.; Pang, Y.; Zhong, M.; Zhang, B.; Li, J.; Chen, P. N.; Zheng, X. L.; Liang, H.; Ge, W. N.; Ye, B. J.; Sinton, D.; Yu, S. H.; Sargent, E. H. Steering Post-C−C Coupling Selectivity Enables High Efficiency Electroreduction of Carbon Dioxide to Multi-Carbon Alcohols. *Nat. Catal.* **2018**, *1*, 421−428.

(25) Zhou, Y.; Che, F.; Liu, M.; Zou, C.; Liang, Z.; De Luna, P. D.; Yuan, H.; Li, J.; Wang, Z.; Xie, H.; Li, H.; Chen, P.; Bladt, E.; Quintero-Bermudez, R.; Sham, T. K.; Bals, S.; Hofkens, J.; Sinton, D.; Chen, G.; Sargent, E. H. Dopant-Induced Electron Localization Drives CO$_2$ Reduction to C$_2$ Hydrocarbons. *Nat. Chem.* **2018**, *10*, 974−980.

(26) Sun, G.; Zhao, Z. J.; Mu, R.; Zha, S.; Li, L.; Chen, S.; Zang, K.; Luo, J.; Li, Z.; Purdy, S. C.; Kropf, A. J.; Miller, J. T.; Zeng, L.; Gang, J. Breaking the Scaling Relationship via Thermally Stable Pt/Cu Single Atom Alloys for Catalytic Dehydrogenation. *Nat. Commun.* **2018**, *9*, 4454.

(27) Darby, M. T.; Réocreux, R.; Sykes, E. C. H.; Michaelides, A.; Stamatakis, M. Elucidating the Stability and Reactivity of Surface Intermediates on Single-Atom Alloy Catalysts. *ACS Catal.* **2018**, *8*, 5038−5050.

(28) Liu, J.; Lucci, F. R.; Yang, M.; Lee, S.; Marcinkowski, M. D.; Therrien, A. J.; Williams, C. T.; Sykes, E. C. H.; Flytzani-Stephanopoulos, M. Tackling CO Poisoning with Single-Atom Alloy Catalysts. *J. Am. Chem. Soc.* **2016**, *138*, 6396−6399.

(29) Kresse, G.; Furthmüller, J. Efficiency of Ab-Initio Total Energy Calculations for Metals and Semiconductors Using a Plane-Wave Basis Set. *Comput. Mater. Sci.* **1996**, *6*, 15−50.

(30) Kresse, G.; Furthmüller, J. Efficient Iterative Schemes for Ab Initio Total-Energy Calculations Using a Plane-Wave Basis Set. *Phys. Rev. B* **1996**, *54*, 11169−11186.

(31) Perdew, J. P.; Burke, K.; Ernzerhof, M. Generalized Gradient Approximation Made Simple. *Phys. Rev. Lett.* **1996**, *77*, 3865−3868.

(32) Blöchl, P. E. Projector Augmented-Wave Method. *Phys. Rev. B: Condens. Matter Mater. Phys.* **1994**, *50*, 17953−17979.

(33) Kresse, G.; Joubert, D. From Ultrasoft Pseudopotentials to the Projector Augmented-Wave Method. *Phys. Rev. B* **1999**, *59*, 1758−1775.

(34) Henkelman, G.; Jónsson, H. Improved Tangent Estimate in the Nudged Elastic Band Method for Finding Minimum Energy Paths and Saddle Points. *J. Chem. Phys.* **2000**, *113*, 9978−9985.

(35) Henkelman, G.; Uberuaga, B. P.; Jónsson, H. A Climbing Image Nudged Elastic Band Method for Finding Saddle Points and Minimum Energy Paths. *J. Chem. Phys.* **2000**, *113*, 9901−9904.

(36) Sanville, E.; Kenny, S. D.; Smith, R.; Henkelman, G. Improved Grid-Based Algorithm for Bader Charge Allocation. *J. Comput. Chem.* **2007**, *28*, 899−908.

(37) Maintz, S.; Deringer, V. L.; Tchougréeff, A. L.; Dronskowski, R. LOBSTER: A Tool to Extract Chemical Bonding from Plane-Wave Based DFT. *J. Comput. Chem.* **2016**, *37*, 1030−1035.

(38) Wang, Y. *VASPMO, version 0.31*, 2016.

(39) Gokhale, A. A.; Dumesic, J. A.; Mavrikakis, M. On the Mechanism of Low-Temperature Water Gas Shift Reaction on Copper. *J. Am. Chem. Soc.* **2008**, *130*, 1402−1414.

(40) Zhao, G.-C.; Wang, J.-S.; Qiu, Y.-Q.; Liu, C.-G. Ensemble Effect of Heterogeneous Cu Atoms Promoting Water-Gas Shift Reaction. *Mol. Catal.* **2020**, *493*, No. 111046.

(41) Zhao, G.-C.; Qiu, Y.-Q.; Liu, C.-G. A Systematic Theoretical Study of Hydrogen Activation Spillover and Desorption in Single-Atom Alloys. *Appl. Catal., A* **2021**, *610*, No. 117948.

(42) Nakamura, J.; Campbell, J.; Campbell, C. T. Kinetics and Mechanism of the Water-Gas Shift Reaction Catalysed by the Clean and Cs-promoted Cu(110) Surface: A Comparison with Cu(111). *J. Chem. Soc., Faraday Trans.* **1990**, *86*, 2725−2734.

(43) Wang, V.; Xu, N.; Liu, J. C.; Tang, G.; Geng, W. T. *VASPKIT: A User-Friendly Interface Facilitating High-Throughput Computing and Analysis Using VASP Code*, arXiv:1908.08269.